



■ BONE BIOLOGY

Accumulation of advanced oxidation protein products contributes to age-related impairment of gap junction intercellular communication in osteocytes of male mice

**C. Tu,
S. Lai,
Z. Huang,
G. Cai,
K. Zhao,
J. Gao,
Z. Wu,
Z. Zhong**

From Nanfang Hospital,
Southern Medical
University, Guangzhou,
China

Aims

Gap junction intercellular communication (GJIC) in osteocytes is impaired by oxidative stress, which is associated with age-related bone loss. Ageing is accompanied by the accumulation of advanced oxidation protein products (AOPPs). However, it is still unknown whether AOPP accumulation is involved in the impairment of osteocytes' GJIC. This study aims to investigate the effect of AOPP accumulation on osteocytes' GJIC in aged male mice and its mechanism.

Methods

Changes in AOPP levels, expression of connexin43 (Cx43), osteocyte network, and bone mass were detected in 18-month-old and three-month-old male mice. Cx43 expression, GJIC function, mitochondria membrane potential, reactive oxygen species (ROS) levels, and nicotinamide adenine dinucleotide phosphate (NADPH) oxidase activation were detected in murine osteocyte-like cells (MLOY4 cells) treated with AOPPs. The Cx43 expression, osteocyte network, bone mass, and mechanical properties were detected in three-month-old mice treated with AOPPs for 12 weeks.

Results

The AOPP levels were increased in aged mice and correlated with degeneration of osteocyte network, loss of bone mass, and decreased Cx43 expression. AOPP intervention induced NADPH oxidase activation and mitochondrial dysfunction, triggered ROS generation, reduced Cx43 expression, and ultimately impaired osteocytes' GJIC, which were ameliorated by NADPH oxidase inhibitor apocynin, mitochondria-targeted superoxide dismutase mimetic (mito-TEMPO), and ROS scavenger N-acetyl cysteine. Chronic AOPP loading accelerated the degradation of osteocyte networks and decreased Cx43 expression, resulting in deterioration of bone mass and mechanical properties *in vivo*.

Conclusion

Our study suggests that AOPP accumulation contributes to age-related impairment of GJIC in osteocytes of male mice, which may be part of the pathogenic mechanism responsible for bone loss during ageing.

Cite this article: *Bone Joint Res* 2022;11(7):413–425.

Keywords: AOPPs, Ageing, Gap junction, Osteocyte, Oxidative stress

Correspondence should be sent to
Zhaoming Zhong; email:
zhongzm@smu.edu.cn

doi: 10.1302/2046-3758.117.BJR-
2021-0554.R2

Bone Joint Res 2022;11(7):413–
425.

Article focus

■ This study aims to investigate the role of the accumulation of advanced oxidation protein products (AOPPs) in the age-related impairment of gap junction intercellular communication (GJIC) in the osteocytes of male mice.

Key messages

- Age-related impairment of GJIC in osteocytes is potentially linked to the accumulation of AOPPs.
- AOPPs induced reactive oxygen species generation and activated nicotinamide adenine dinucleotide phosphate oxidase

signalling pathway in osteocytes, which is a potential mechanism for impairment of osteocytes' GJIC and degeneration of cortical bone.

Strengths and limitations

- To our knowledge, our study demonstrated firstly the effect of AOPP accumulation on osteocyte GJIC and degeneration of cortical bone in aged male mice.
- The effect of AOPP accumulation on the osteocyte network in aged female mice requires further investigation.

Introduction

Osteocytes represent 90% to 95% of all bone cells in the adult skeleton, are embedded within the bone mineral matrix, and have a highly dendritic morphology.¹ The long dendritic processes of osteocytes form a lacuno-canalicular network connecting the neighbouring osteocytes and the cells on the bone surface, such as osteoblasts and osteoclasts.^{2,3} Gap junctions are formed at the connection site between two dendrites of neighbouring cells and allow cell-to-cell communication to exchange small molecules (< 1 kDa).⁴ This exchange is known as the gap junctional intercellular communication (GJIC).⁵ Osteocytes play a critical role in regulating skeletal homeostasis, orchestrating osteoblasts and osteoclasts via GJIC.^{6,7} Emerging evidence shows that ageing is associated with loss of osteocyte dendricity and degeneration of the lacuno-canalicular network, which further impairs GJIC.⁸⁻¹⁰ Age-related impairment of GJIC in osteocytes contributes to the deterioration of bone quality and bone mass.¹¹

Connexins are the main structural proteins of gap junctions.¹² A hexameric array of six connexin subunits forms a hemichannel.¹³ Each apposed cell contributes a hemichannel to the formation of a complete channel, the gap junction.¹⁴ So far, at least 20 connexin isoforms in humans and mice have been reported.¹⁵ Among them, connexin43 (Cx43) shows the most abundant expression in osteocytes.¹⁶ GJIC is mediated by connexins, in particular Cx43.¹⁷ Cx43 mediated GJIC is essential for the survival of osteocytes and bone remodelling.¹⁸ It has been demonstrated that Cx43 expression is decreased in osteocytes from aged mice compared to young mice.⁹ Oxidative stress acts as a key contributor to ageing. Two studies have shown that oxidative stress results in decreased Cx43 expression, accompanied by the impairment of GJIC, which is responsible for age-related bone loss and osteoporosis.^{9,17}

Advanced oxidation protein products (AOPPs) are dityrosine-containing protein crosslinking products formed during oxidative stress.¹⁹ The plasma level of AOPPs is significantly higher in elderly people in comparison with adults and children/adolescents.²⁰ Accumulation of AOPPs is also observed in patients with osteoporosis.²¹ Research has demonstrated that AOPP accumulation is associated with the deterioration of bone microstructure and bone loss in aged mice.^{22,23} AOPPs are

not only a marker of oxidative stress but also a trigger of oxidative stress. Previous studies have indicated that AOPPs induce generation of reactive oxygen species (ROS) and redox imbalance, affecting diverse cellular functions such as proliferation,²⁴ differentiation,²⁵ apoptosis,²² inflammation,²⁶ and autophagy.²⁷ However, the effect of AOPP accumulation during ageing on the osteocyte GJIC remains unclear.

In this study, we demonstrate that AOPP accumulation is correlated with the impairment of osteocyte GJIC and bone loss in aged male mice. AOPP intervention reduced osteocyte dendrites and Cx43 expression, and impaired osteocytes' GJIC through disruption of redox homeostasis.

Methods

Preparation and detection of AOPPs. AOPPs were prepared as described by a previous study.²² Briefly, the mouse serum albumin (MSA) solution (20 mg/ml; Merck, USA) was mixed with an equal volume of hypochloric acid solution (40 mM; Fluka, Switzerland), and the reaction was carried out in darkness at room temperature for 30 minutes. The prepared samples were then transferred to a dialysis bag and free hypochloric acid was removed with phosphate-buffered saline (PBS, pH = 7.4). To remove contaminated endotoxin, all samples were passed through a Detoxi-Gel column (Thermo Fisher Scientific, USA). Quantitation of AOPPs was performed according to the previous description.²⁸ In brief, 200 µl of sample or chloramine-T was added into a 96-well plate separately, then mixed with 10 µl potassium iodide (KI) and 20 µl acetic acid, and the absorbance at 340 nm was measured immediately in the microplate reader (Molecular Devices, USA). AOPP concentrations were expressed as mmol/l (plasma) or nmol/mg protein (femur) of chloramine-T equivalents.

Animal experiments. Both three-month-old and 18-month-old male C57BL/6 J mice were purchased from the Animal Experimental Center of Nanfang Hospital, Southern Medical University. The animals were housed six per cage and maintained at a controlled room temperature (22°C ± 2) on a 12-hour light/dark cycle. Food and water were available ad libitum. All animals were allowed to adapt to the environment for a week and were then killed by an intraperitoneal injection of pentobarbital sodium (0.5 mg/kg). Blood samples and lower limbs were collected and stored at -80°C for further study, and right lower limbs were collected and fixed in 4% paraformaldehyde.

In identical experiments, the three-month-old male mice were randomly divided into the following four groups (n = 6 in each group) in a completely randomized manner: 1) control group – daily intraperitoneal injection of vehicle (PBS, pH = 7.4); 2) MSA group – daily intraperitoneal injection of unmodified MSA (50 mg/kg); 3) AOPPs group – daily intraperitoneal injection of AOPPs (50 mg/kg); and 4) AOPPs + NAC group – daily intraperitoneal injection of AOPPs (50 mg/kg) together with

N-acetylcysteine (NAC, a free radical scavenger) at 2 mg/kg in drinking water. After 12 weeks of administration, all animals were killed and the samples were collected as described above. Animal studies were conducted in line with the ARRIVE guidelines; an ARRIVE checklist is included in the Supplementary Material accordingly.

Cell culture. Murine osteocyte-like cells (MLOY4 cells) were obtained from the Committee of Type Culture Collection, and grown on collagen-coated dishes in Dulbecco's modified Eagle's medium (DMEM; Gibco, USA) containing 10% fetal bovine serum (FBS, Gibco) and 1% penicillin-streptomycin (Gibco) at 37°C in a humidified atmosphere with 5% CO₂, as reported in a previous study.²⁹ After two days, the cells reached a confluent state and were subcultured.

Visualization of the osteocyte network. Visualization of the osteocyte network was performed as described previously.⁸ Briefly, all femora were removed and fixed in 4% paraformaldehyde overnight at 4°C, then decalcified with 10% ethylenediaminetetraacetic acid (EDTA) for three weeks and embedded with paraffin. Serial transverse sections were cut at 30 µm thickness using a Leica cryomicrotome (Leica Microsystems, Germany). Sections were permeabilized with 1% Triton X-100 (Beyotime, China) for 15 minutes, blocked with 5% goat serum for one hour, and then incubated in tetramethylrhodamine (TRITC)-conjugated phalloidine (1:200, Yeasen Biotechnology, China) overnight followed by three PBS washes. Nuclei were counterstained with 4,6-diamidino-2-phenylindole (DAPI; Abcam, UK).

For confocal imaging, the images were obtained by FV3000 confocal fluorescence microscopy (Olympus, Japan). A tiled image of the slice was obtained with the ten-fold objective magnification followed by collecting detailed Z-stacks of 250 to 350 Z-planes with the 100× oil objective lens (NA 1.44 zoom 1.7 with a 0.23 µm step size). The phalloidin images were acquired by 555 nm laser excitation.

Western blot. The cells and bone samples were homogenized in ice-cold radioimmunoprecipitation assay (RIPA) buffer with 1 mM phenylmethylsulfonyl fluoride (PMSF), protease and phosphatase inhibitors. The supernatant was centrifuged at 4°C, 12,000 rpm for 20 minutes to extract the protein. Protein concentration was detected by bicinchoninic acid (BCA) assay kit (Beyotime). The samples were separated by electrophoresis on a 10% sodium dodecyl sulfate (SDS)-polyacrylamide gel (PAGE), and then transferred to polyvinylidene fluoride (PVDF) membranes (Merck, USA). The membranes were blocked with 5% nonfat dry milk in Tris-buffered saline (Merck) with 0.1% TWEEN 20 (Merck) for one hour at room temperature, then they were probed overnight with the following primary antibodies: rabbit anti-Cx43 (1:2,000, Abcam, UK), rabbit anti-nicotinamide adenine dinucleotide phosphate (NADPH) oxidase 1 (NOX1; 1:800, Proteintech, China), rabbit anti-NADPH oxidase 2 (NOX2; 1:800, Proteintech), and rabbit anti-NADPH oxidase 4 (NOX4; 1:800, Proteintech). The membrane

was washed three times with TBST for ten minutes, then incubated with the appropriate secondary antibody for one hour, followed by another three washes in TBST, and rabbit anti-glyceraldehyde 3-phosphate dehydrogenase (GAPDH) (1:5,000, Merck, USA) was used as an internal control for tissue samples. After incubation with primary and secondary antibodies, detection of protein bands with enhanced chemiluminescence detection reagents (Beyotime) was conducted.

Micro-CT analysis. The right femur was fixed with 4% paraformaldehyde for at least 24 hours and then scanned with a micro-CT system (µCT80, Scanco Medical, Switzerland). All samples were scanned with a nominal resolution of 12 µm, a source voltage of 80 kV, and a tube current of 0.1 mA. The volume of interest (VOI) of the two regions (middle and distal scan regions of the femur) was defined as 100 layers of the distal and middle femur. Two VOIs were chosen for cortical bone and distal cancellous bone analysis. Reconstructed 3D images were analyzed with CTvox software. The cortical bone parameters, such as total cortical bone area (Tt.Ar), average cortical area (Ct.Ar), cortical bone thickness (Ct.Th), and the parameters of the trabecular bone microstructure, such as bone mineral density (BMD), bone volume/total volume (BV/TV), trabecular thickness (Tb.Th), trabecular number (Tb.N), and trabecular spacing (Tb.Sp), were calculated.

Mechanical three-point bending test. Three-point bending tests were performed to evaluate the mechanical quality of the tibia of mice, using a materials testing machine (ElectroPuls E1000, Instron, USA) with a load cell of 100 N. The posterior side of the fresh tibia was placed down between two frames spanning 10 mm. A preload of 0.5 N was applied to the midpoint of the tibia to maintain the tibia in position. A compressive force was applied to the tibia at a 2 mm/min rate. The test was stopped automatically in case of failure or displacement greater than 2 mm. The maximum bending force and stiffness were calculated from the force-displacement curves.

Immunofluorescence staining. Immunofluorescence staining was performed as described previously.²² Briefly, MLOY4 cells were cultured in 35 mm confocal dishes at a density of 2×10^5 cells/dish for 24 hours. They were then fixed in 4% paraformaldehyde for 15 minutes, rinsed with PBS three times, permeabilized with 0.5% Triton X-100 (Beyotime) for 15 minutes, and blocked with 5% goat serum for one hour. The samples were then incubated with the anti-Cx43 rabbit monoclonal antibody (1:1,000, Abcam, UK) overnight at 4°C. The secondary antibody was fluorescein isothiocyanate (FITC) fluorescent antibody (1:1,000, Abcam, UK) and TRITC-conjugated phalloidine (1:200, Yeasen Biotechnology), which was used to label the cytoskeleton. Nuclei were counterstained with DAPI (Abcam, UK).

The optimal cutting temperature (OCT) compound embedded femur was sliced into 10 µm-thick transverse sections. The slices were incubated with primary antibodies against voltage-dependent anion channels (VDAC) (1:1,000, Abcam, UK) at 4°C overnight. The secondary antibody was CY5 fluorescent antibody (1:1,000, Abcam,

UK), and the slides were sealed by mounting medium with DAPI. Images were captured with a contained confocal laser scanning microscope system (Olympus).

Immunohistochemical staining. Paraffin embedded bone tissue was sliced into 5 μm -thick transverse sections. The paraffin sections were deparaffinized in toluene, rehydrated through degraded ethanol, and then rinsed twice with distilled water. The slides were placed in 0.01 M citrate buffer to retrieve antigen. Then the slides were blocked with 5% BSA and 0.3% Triton X-100 (Yeasen Biotechnology) for 60 minutes, and incubated with the antibody anti-Cx43 (1:800, Abcam, UK) at 4°C overnight followed by the goat anti-rabbit antibody (1:1,000, Abcam, UK) for 60 minutes. The immunostaining was examined by a Leica DM5000B microscope (Leica).

ROS detection. Intracellular ROS level was detected by the fluorescent probe 2',7'-dichlorofluorescein diacetate (DCFH-DA) (Beyotime) according to the manufacturer's instruction. Briefly, the MLOY4 cells were incubated with 10 μM DCFH-DA for 20 minutes in the dark incubator at 37°C. Fluorescence intensity (Ex/Em = 488/525) was measured on a SpectraMax M5 system (Molecular Devices) and visualized with IX73 fluorescence microscopy (Olympus).

Moreover, the mitochondrial superoxide level was determined by MitoSOX Red mitochondrial superoxide indicator (Thermo Fisher Scientific). In brief, MLOY4 cells were incubated with 5 μM MitoSOX reagent stock solution for ten minutes in the dark incubator at 37°C. MitoSOX fluorescence intensity (Ex/Em = 510/580) was measured on a SpectraMax M5 system (Molecular Devices), and observed with IX73 fluorescence microscopy.

Mitochondrial membrane potential assay. Mitochondrial membrane potential was determined with fluorescent lipophilic carbocyanine dye JC-1 (KeyGen Biotech, China). In brief, MLOY4 cells were seeded in the confocal dish, and incubated with a mixture of 2 μl JC-1, 900 μl double distilled H₂O (ddH₂O), and 100 μl incubation buffer for 20 minutes in the dark incubator at 37°C. The incubation solution was then removed, and cells were washed twice with incubation buffer and observed with an IX73 fluorescence microscope.

Scrape loading and dye transfer assay. The scrape loading and dye transfer assay were used to assess GJIC as described previously.³⁰ Briefly, cells were seeded in six-well dishes at a density of 2×10^5 cells/dish for 24 hours. The fully confluent cells were washed with PBS, then scraped using a surgical blade prior to the addition of Lucifer Yellow (LY) fluorescent dye (1 mg/ml) (Merck). After incubating at room temperature for seven minutes, cells were washed with PBS three times and observed with the IX73 fluorescence microscope.

Statistical analysis. All experiments were repeated at least three times. Continuous variables were presented as mean and standard deviation (SD). One-way analysis of variance (ANOVA) was used for multiple comparisons, and p-values less than 0.05 between groups were

considered statistically significant. Statistical analyses were conducted with SPSS 22.0 software (IBM, USA).

Results

Accumulation of AOPPs was correlated with the impairment of osteocyte GJIC in aged male mice. To clarify the correlation between AOPPs accumulation during ageing and GJIC in osteocytes, experiments were performed in three- and 18-month-old male mice. As shown in Figures 1a and 1b, the levels of AOPPs in plasma and bone tissue were significantly higher in aged mice than those in young mice. As shown in Figure 1c, compared to young mice, the aged mice showed degeneration of the osteocyte network, including loss of dendritic processes in a single cell and decreased gap junctions between adjacent osteocytes. As shown in Figures 1d and 1e, the expression of Cx43 in bone tissue of aged mice was significantly lower than that in young mice. We also examined VDAC in osteocytes of mice, a marker recognized for evaluating total mitochondrial mass.³¹ As shown in Figure 1f, the VDAC expression in osteocytes of aged mice was significantly lower than that of young mice. Furthermore, the micro-CT analyses showed the deterioration of bone microstructure and low bone mass in aged mice (Figures 2a to 2l). The maximum bending stress and stiffness were significantly lower in aged mice compared to young mice (Figures 2m and 2n).

AOPPs impaired the GJIC in osteocytes in vitro. To determine the effect of AOPPs on GJIC of osteocytes, MLOY4 cells were treated with or without AOPPs. First, the scrape loading/dye transfer assay was performed to assess GJIC. As shown in Figures 3a and 3b, after loading of LY, the dye transmission speed among the living osteocytes was slower during the initial seven minutes in the AOPP-treated group compared with the control group. Next, we analyzed the expression of hemichannel protein Cx43. As shown in Figures 3c to 3e, the immunofluorescence staining showed that dot-like distributions of Cx43 were barely present in cell processes and cytoplasm after AOPP intervention, and the western blot showed that AOPP treatment resulted in greatly diminished expression of Cx43 in a dose- and time-dependent manner.

AOPPs induce ROS generation through NADPH oxidase and mitochondrial pathways. To examine whether AOPPs induced ROS generation and redox imbalance in osteocytes, we determined the intracellular ROS level by the fluorescent 2',7'-dichlorofluorescein diacetate (DCFH-DA) probe and mitochondrial superoxide level by MitoSOX Red staining in MLOY4 cells. As shown in Figures 4a to 4d, AOPP intervention induced the generation of intracellular ROS and mitochondrial superoxide in a dose- and time-dependent manner. NADPH oxidase and mitochondria play a pivotal role in intracellular ROS homeostasis.^{32,33} As shown in Figures 4e to 4i, AOPP treatment resulted in an increased expression of NADPH oxidase 2 (NOX2) and NADPH oxidase 4 (NOX4), and

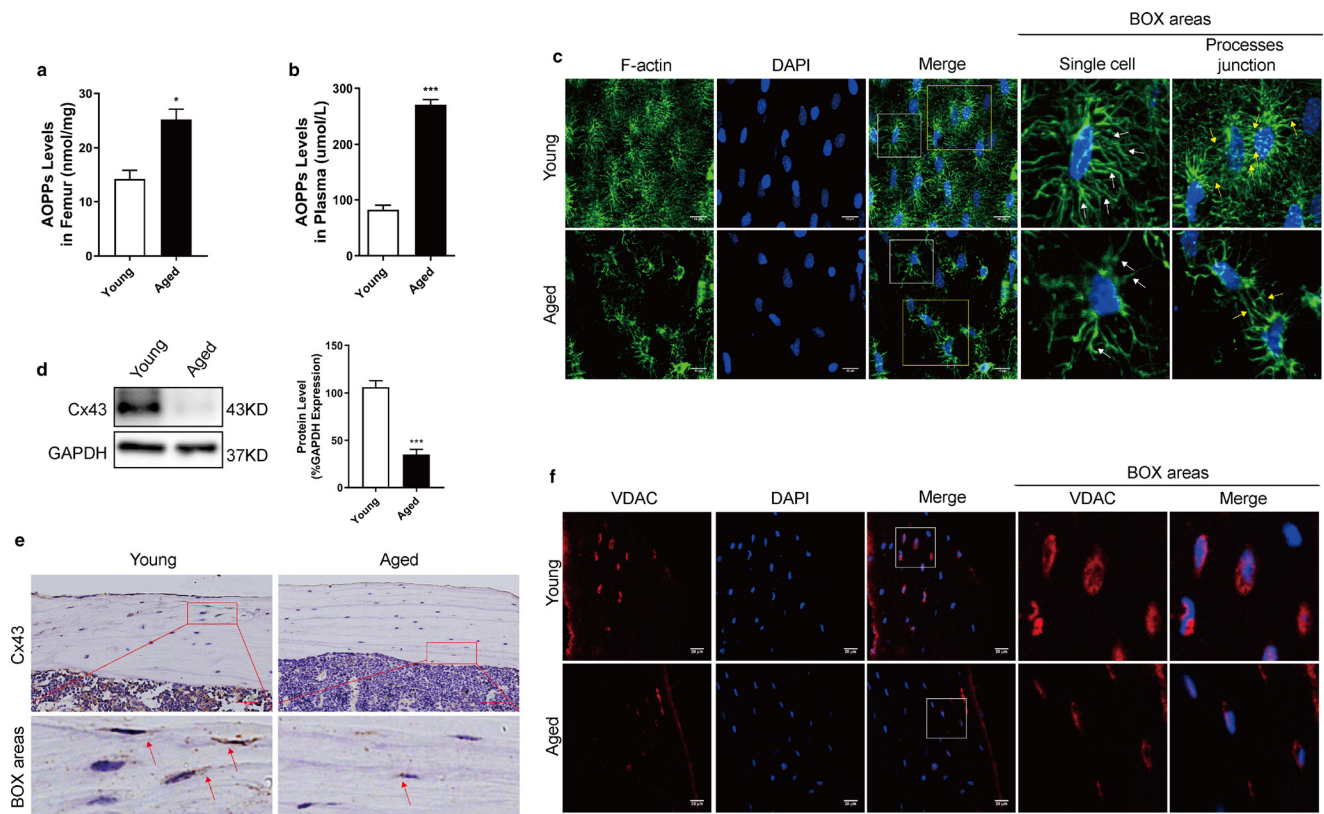


Fig. 1

Advanced oxidation protein product (AOPP) accumulation and disruption of osteocyte gap junction intercellular communication (GJIC) with ageing. a) The levels of AOPPs increased in femur of aged male mice ($n = 6$ ageing, $n = 6$ young). b) The levels of AOPPs increased in plasma of aged male mice ($n = 6$ ageing, $n = 6$ young). c) Representative confocal microscope image of the number of dendritic processes in a single cell (white arrow) and gap junctions between adjacent osteocytes (yellow arrow) stained by phalloidin (bar = 10 μm). d) and e) In immunohistochemical staining of anti-connexin43 (Cx43) antibody, decreased expression of Cx43 was shown in femur cortical bone of aged male mice (bar = 20 μm). f) Mitochondrial mass was labelled for voltage-dependent anion channel (VDAC, red); VDAC expression was decreased in osteocytes of aged male mice (bar = 20 μm), nuclei were stained with 4,6-diamidino-2-phenylindol (DAPI) (blue). Data are represented as means (standard error of the mean (SEM)). * $p < 0.05$, *** $p < 0.001$ versus control group. GAPDH, glyceraldehyde 3-phosphate dehydrogenase. BOX area, enlarged image of the box area of merge images in Figures 1c, 1e, and 1f.

resulted in the loss of mitochondrial membrane potential ($\Delta\Psi\text{m}$) in a dose- and time-dependent manner in MLOY4 cells (JC-1 aggregate represents normal $\Delta\Psi\text{m}$, JC-1 monomer represents decreased $\Delta\Psi\text{m}$).

In order to further confirm the pathway of AOPPs inducing ROS generation, we pretreated cells with NADPH oxidase inhibitors (apocynin), mitochondria-targeted superoxide dismutase mimetic (mito-TEMPO), and radical scavenger N-acetylcysteine (NAC). As shown in Figures 4j and 4k, the presence of apocynin, mito-TEMPO, and NAC significantly ameliorated the intracellular ROS generation induced by AOPPs.

ROS signalling involved in AOPP-induced impairment of GJIC in osteocytes. To elucidate the effect of ROS generation induced by AOPPs on the impairment of osteocyte GJIC, the MLOY4 cells were pretreated with apocynin, mito-TEMPO, and NAC. As shown in Figures 5a and 5b, after pretreatment with apocynin, mito-TEMPO, and NAC, the dye transmission speed in the living osteocytes was significantly faster than that in cells with only AOPP intervention. As shown in Figures 5c and 5d, AOPPs decreased expression of Cx43, an effect which

was reversed by pretreatment with apocynin, mito-TEMPO, and NAC.

Chronic AOPPs loading accelerated the impairment of osteocyte GJIC in vivo. To further demonstrate the effect of AOPPs on osteocyte GJIC, the young male mice were injected intraperitoneally with AOPPs for 12 weeks. Chronic AOPP loading resulted in loss of dendritic processes in a single cell, decreased gap junctions between adjacent osteocytes (Figure 6a), and reduced expression of Cx43 in osteocytes (Figures 6b and 6c). Conversely, the presence of NAC (2 mg/kg) reversed the degeneration of the osteocyte network and decreased expression of Cx43 induced by AOPPs (Figures 6a to 6c). The micro-CT analyses showed that chronic AOPP loading accelerated the deterioration of bone microstructure and loss of bone mass, which were reversed by treatment with antioxidant NAC (Figures 7a to 7l). AOPP intervention reduced the maximum bending stress and stiffness of the tibia, which were improved by NAC treatment (Figures 7m and 7n).

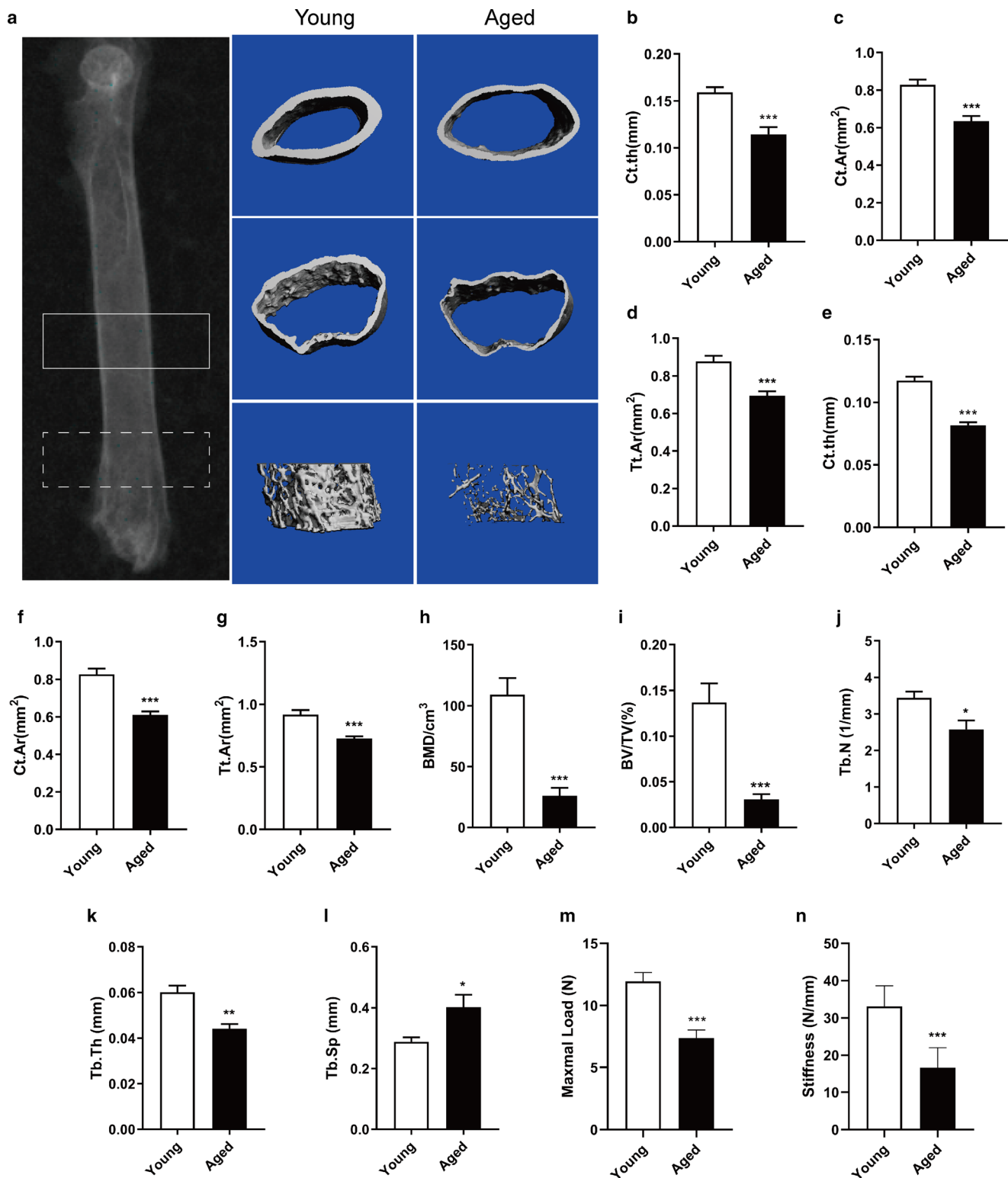


Fig. 2

Deterioration of bone microstructure and mechanical properties in aged mice. a) The cortical bone of middle femur (solid line) and the cortical and cancellous bone of distal femur (dotted lines) were reconstructed by 3D micro-CT ($n = 6$ ageing, $n = 6$ young). b) to d) Cortical bone thickness (Ct.th), average cortical bone area (Ct.Ar), and total cortical bone area (Tt.Ar) were diminished in the middle femur in aged male mice. e) to g) Ct.th, Ct.Ar, and Tt.Ar were decreased in the distal femur in aged mice. h) to l) Bone mineral density (BMD), bone volume/total volume (BV/TV), trabecular number (Tb.N), and trabecular thickness (Tb.Th) decreased, and trabecular spacing (Tb.Sp) increased in cancellous bone in aged mice. m) and n) Maximal bending stress and stiffness were decreased in the tibia in aged male mice ($n = 6$ ageing, $n = 6$ young). Data are represented as means (standard error of the mean (SEM)). * $p < 0.05$, ** $p < 0.01$, *** $p < 0.001$ versus young group.

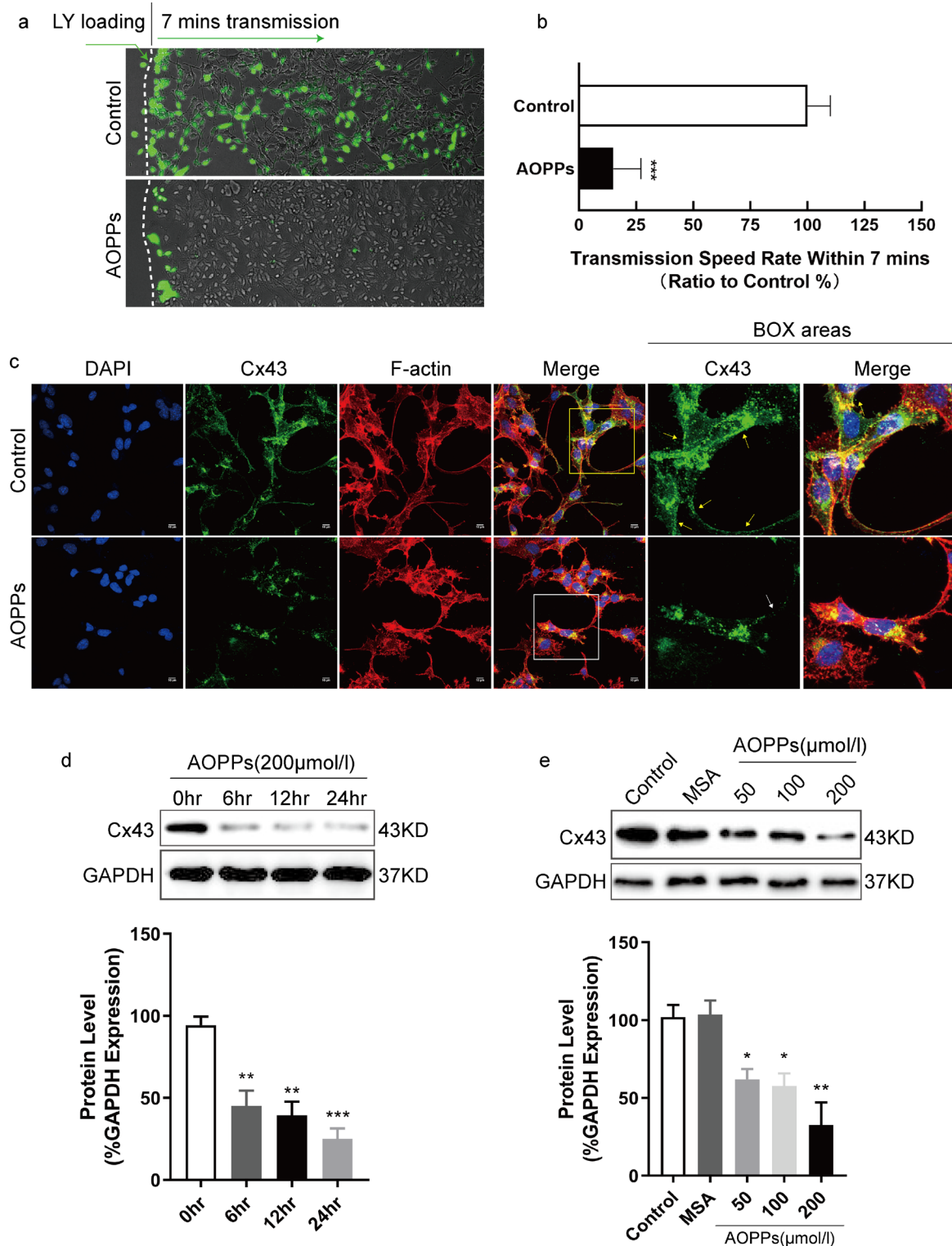


Fig. 3

Advanced oxidation protein products (AOPPs) disrupt the gap junction intercellular communication (GJIC) in murine osteocyte-like cells (MLOY4 cells). a) and b) The scrape loading/dye transfer assay showed that AOPP intervention resulted in decreased Lucifer Yellow (LY, green) transmission speed among the living MLOY4 cells ($n = 3$ independent experiments), original magnification: 10 \times objective. c) Representative confocal microscope image of the expression and distribution of connexin43 (Cx43, green) in the dendritic processes and cytoplasm of MLOY4 cells (bar = 10 μ m) ($n = 3$ independent experiments), nuclei were stained with 4,6-diamidino-2-phenylindole (DAPI, blue). d) and e) The expression of Cx43 was diminished by AOPPs (0 to 200 μ mol/l, 0 to 24 hrs) in a time-dependent and dose-dependent manner ($n = 3$ independent experiments). Data are represented as means (standard error of the mean (SEM)). * $p < 0.05$, ** $p < 0.01$, *** $p < 0.001$ versus control group. GAPDH, glyceraldehyde 3-phosphate dehydrogenase; MSA, mouse serum albumin. BOX area, enlarged image of the box area of merge images in Figure 3c.

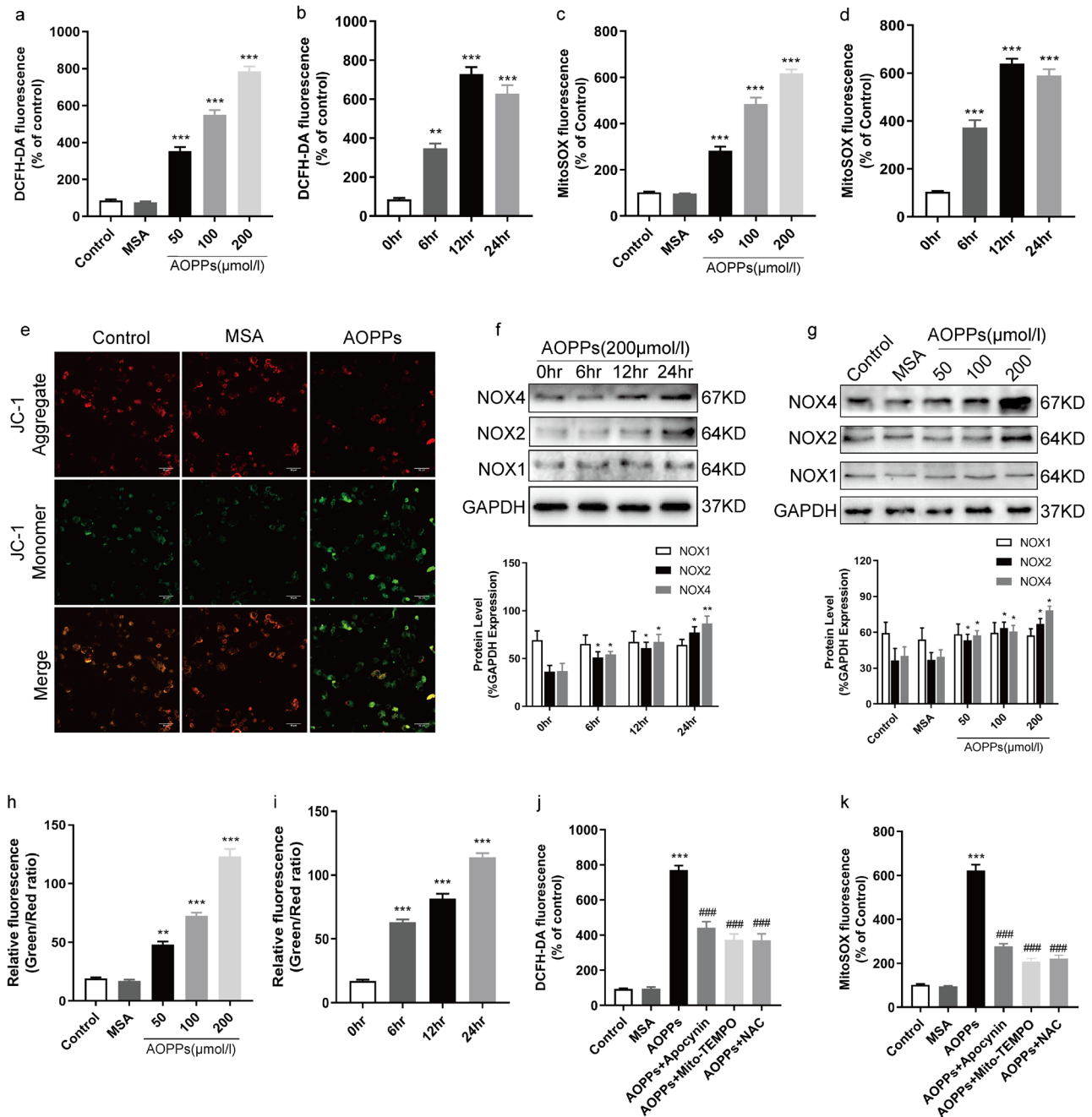


Fig. 4

Advanced oxidation protein products (AOPPs) induced reactive oxygen species (ROS) generation through nicotinamide adenine dinucleotide phosphate (NADPH) oxidase and mitochondrial pathways. a) and b) 2',7'-dichlorofluorescein diacetate (DCFH-DA) fluorescent probe assay showed that AOPPs induced intracellular ROS generation in a dose- and time-dependent manner ($n = 5$ independent experiments). c) and d) MitoSOX Red staining showed that AOPPs induced mitochondrial superoxide generation in a dose- and time-dependent manner ($n = 5$ independent experiments). e) A confocal laser scanning microscope system was used to visualize loss of mitochondrial membrane potential ($\Delta\Psi_m$) level in murine osteocyte-like cells (MLOY4) cells with the use of JC-1 staining. JC-1 aggregate (red) represents normal $\Delta\Psi_m$, JC-1 monomer (green) represents decreased $\Delta\Psi_m$ (bar = 50 μm) ($n = 3$ independent experiments). f) and g) AOPPs (0 to 200 $\mu\text{mol/l}$, 0 to 24 hrs) significantly augmented NADPH oxidase 2 (NOX2) and NADPH oxidase 4 (NOX4) expression in a time-dependent and dose-dependent manner in MLOY4 ($n = 3$ independent experiments). h) and i) Numerical data were expressed in terms of the ratio of JC-1 aggregates to JC-1 monomers. j) and k) AOPP-induced (200 $\mu\text{mol/l}$, 12 hr) intracellular total and mitochondrial ROS generation was declined by apocynin, mitochondria-targeted superoxide dismutase mimetic (mito-TEMPO), and N-acetylcysteine (NAC). Data are represented as means (standard error of the mean (SEM)). * $p < 0.05$, ** $p < 0.01$, *** $p < 0.001$ versus control group or 0 hr group; ### $p < 0.001$ versus AOPPs group. GAPDH, glyceraldehyde 3-phosphate dehydrogenase; MSA, mouse serum albumin.

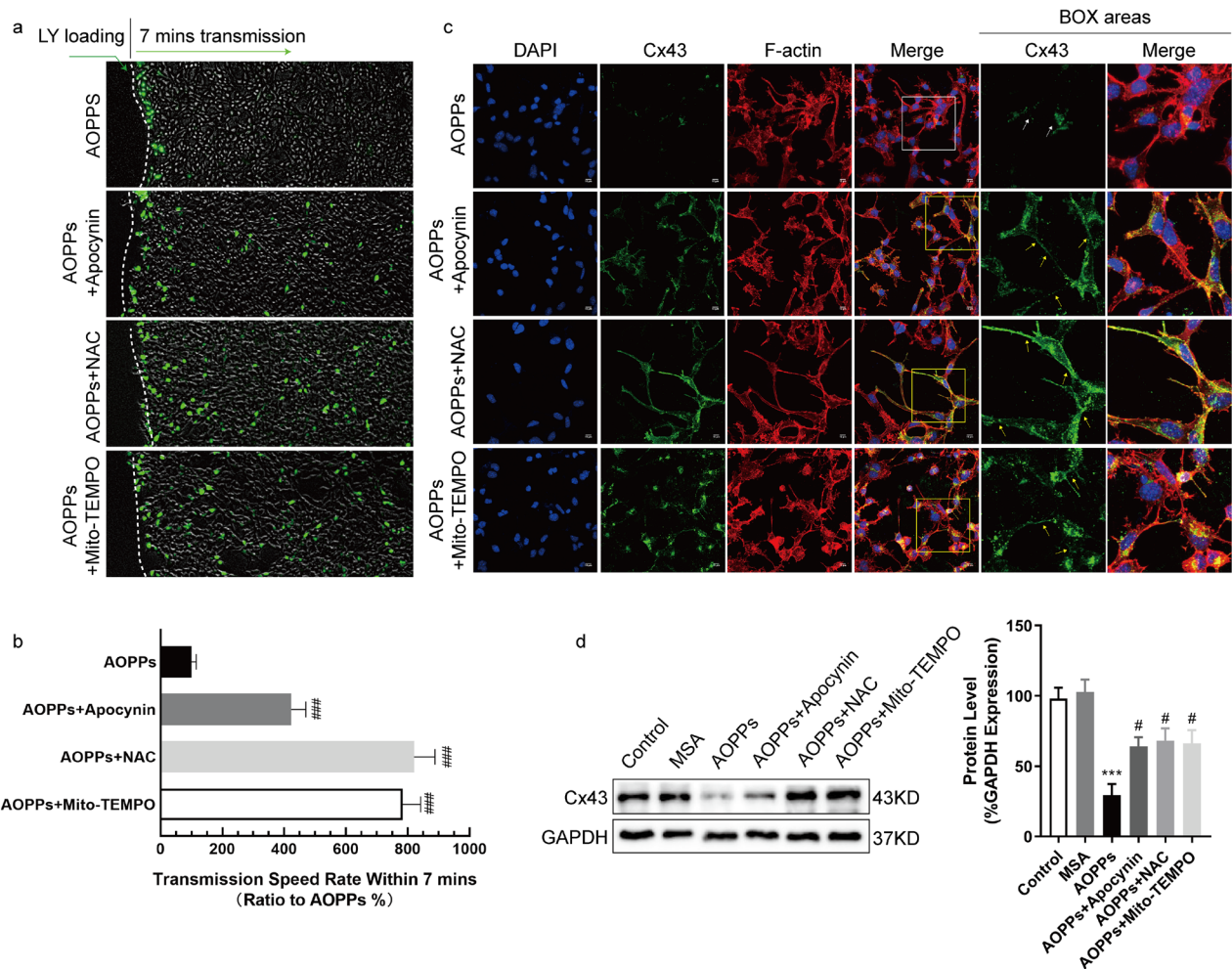


Fig. 5

Reactive oxygen species (ROS) signalling involved in advanced oxidation protein product (AOPP)-induced disruption of gap junction intercellular communication (GJIC) in murine osteocyte-like cells (MLOY4 cells). a) and b) The scrape loading/dye transfer assay showed that the transmission speed of Lucifer Yellow (LY, green) was increased after pretreatment with apocynin, mitochondria-targeted superoxide dismutase mimetic (mito-TEMPO), and N-acetylcysteine (NAC) ($n = 3$ independent experiments); original magnification: 10 \times objective. c) Representative confocal microscope image of the expression and distribution of connexin43 (Cx43, green) in dendritic processes and cytoplasm of MLOY4 cells (bar = 10 μ m) ($n = 3$ independent experiments); nuclei were stained with 4,6-diamidino-2-phenylindole (DAPI, blue). d) AOPPs decreased expression of Cx43, an effect which was reversed by pretreatment with apocynin, mito-TEMPO, and NAC ($n = 3$ independent experiments). Data are represented as means (standard error of the mean (SEM)). *** $p < 0.001$ versus control group; # $p < 0.05$, ### $p < 0.001$ versus AOPPs group. GAPDH, glyceraldehyde 3-phosphate dehydrogenase; MSA, mouse serum albumin. BOX area, enlarged image of the box area of merge images in Figure 5c.

Discussion

Bone is a dynamic tissue, and bone homeostasis is maintained by numerous cells and factors.^{34,35} GJIC in osteocytes plays a critical role in regulating signal transmission among different bone cells and maintaining bone homeostasis.^{6,7,36} Emerging evidence has shown that osteocyte GJIC is impaired during the ageing process, which is closely associated with elevated levels of oxidative stress.^{8,17} AOPPs accumulate with age and involve a variety of cellular pathological processes.^{22,37-39} In the current study, we confirmed that AOPP accumulation during ageing contributed to the impairment of GJIC in osteocytes.

Gap junction channels, located at the tips of the osteocyte cell processes and consisting of connexin, especially Cx43, are responsible for GJIC in the osteocyte network.^{12,18} Osteocyte GJIC plays a critical role in integrating environmental cues, including essential nutrients, survival factors, and mechanical stimuli. In this study, we observed more decreased expression of Cx43, increased degeneration of the cortical bone, and increased impairment of the osteocyte network in aged mice compared with young mice. These results indicate that ageing is related to the degeneration of the osteocyte network and decrease of Cx43 expression, which may impair the osteocyte GJIC. It has been

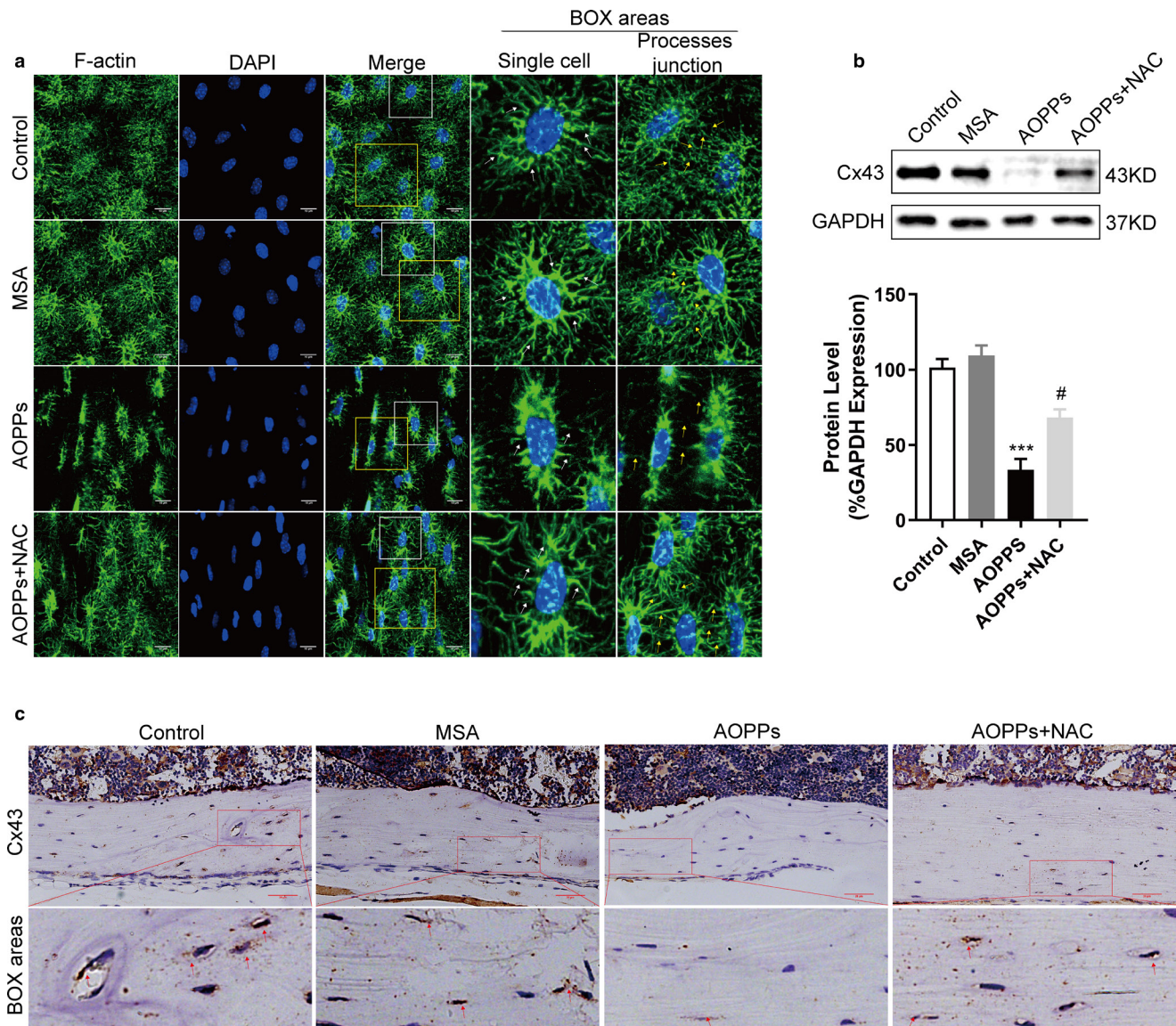


Fig. 6

Chronic advanced oxidation protein product (AOPP) loading accelerated the impairment of gap junction intercellular communication (GJIC) in osteocytes in vivo. a) Representative confocal microscope images showed that chronic AOPP loading accelerated the loss of dendritic processes in a single cell and decreased gap junctions among adjacent osteocytes (bar = 10 μ m); osteocyte was labelled with phalloidine (green), nuclei were stained with 4,6-diamidino-2-phenylindole (DAPI, blue). b) and c) In immunohistochemical staining and western blot of anti-Cx43 antibody, chronic AOPP loading reduced expression of connexin43 (Cx43) (bar = 20 μ m). Furthermore, the antioxidant N-acetylcysteine (NAC) could alleviate the degeneration of osteocyte network and decreased Cx43 expression induced by AOPPs (a) to c). Data are represented as means (standard error of the mean (SEM)), six mice in each group were analyzed. ***p < 0.01, ****p < 0.001 versus control group; #p < 0.05, ##p < 0.01 versus AOPPs group. DAPI, 4,6-diamidino-2-phenylindole; GAPDH, glyceraldehyde 3-phosphate dehydrogenase; MSA, mouse serum albumin. BOX area, enlarged image of the box area of merge images in Figures 6a and 6c.

demonstrated that the impairment of osteocyte GJIC is a major factor for the reduction of Ct.Th and bone strength in the elderly.^{10,40} We also discovered deterioration of bone microstructure and low bone mass in aged male mice, and the maximum bending stress and stiffness in aged male mice were lower than in young male mice. Therefore, age-related impairment of osteocyte GJIC may be involved in bone loss.

AOPPs are an endogenous marker of oxidative stress. Ageing is accompanied by enhanced oxidative stress and AOPP accumulation.^{41,42} In this study, we observed

that the levels of AOPPs in plasma and bone tissues were increased in aged mice compared with young mice. AOPPs also serve as a pathogenic factor by triggering ROS generation and disrupting redox homeostasis. Previous studies have shown that AOPPs induce the osteoblast apoptosis and neuro inflammation through oxidative stress.^{22,39,43} Emerging evidence shows that oxidative stress is instrumental in the impairment of osteocyte networks, and hydrogen peroxide (H_2O_2) treatment decreases Cx43 expression and GJIC in osteocytes.^{9,17} We observed that AOPP intervention resulted

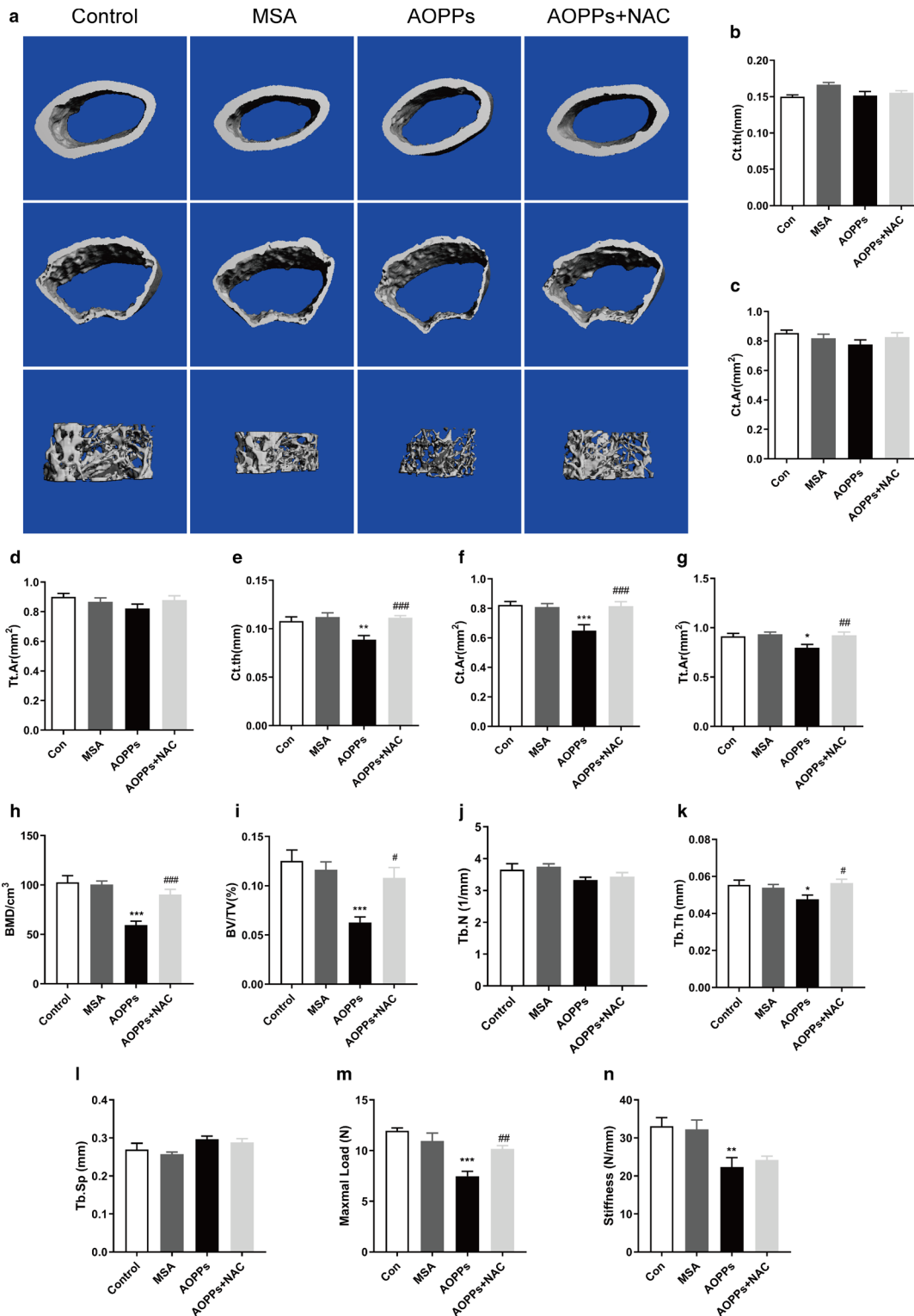


Fig. 7

Chronic advanced oxidation protein product (AOPP) loading deteriorated bone microstructure and mechanical properties. a) 3D micro-CT reconstruction and cross-sectional images showed that AOPP administration used a severe deterioration to bone microstructure of cortical and cancellous of distal femur, original magnification: 50x. b) to d) Chronic AOPP treatment has no effect on cortical bone thickness (Ct.th), average cortical bone area (Ct.Ar), or total cortical bone area (Tt.Ar) in middle cortical bone. e) to g) AOPP loading decreased the Ct.th, Ct.Ar, and Tt.Ar in distal cortical femur. h) to l) Chronic AOPP loading decreased bone mineral density (BMD), bone volume/total volume (BV/TV), and trabecular thickness (Tb.Th), but there was no change in trabecular number (Tb.N) and trabecular spacing (Tb.Sp) in distal cancellous femur. m) and n) Chronic AOPP loading reduced maximal bending stress and stiffness in tibia, which was reversed by N-acetylcysteine (NAC) treatment. Data are represented as means (standard error of the mean (SEM)), and six mice in each group were analyzed. *p < 0.05, **p < 0.01, ***p < 0.001 versus control group; #p < 0.05, ##p < 0.01, ###p < 0.001 versus AOPP group. Con, control.

in an increase of intracellular ROS, decrease of Cx43 expression, loss of dendritic processes in a single cell, and decreased gap junctions between adjacent osteocytes. AOPP loading resulted in degradation of cortical bone of mice, and decreased mechanical properties and bone mass. Furthermore, AOPPs slow the dye transmission speed among the living osteocytes, which directly indicates the impairment of GJIC among osteocytes. Therefore, we hypothesized that AOPP accumulation could play an important role in age-related impairment of osteocyte GJIC.

Mitochondria are one of the primary sources of ROS. Mitochondrial quality and activity have been associated with ageing and correlated with the development of a wide range of age-related diseases. We observed that the expression of VDAC, a marker of mitochondrial mass, was lower in osteocytes of ageing male mice compared with young male mice. Normal mitochondrial membrane potential (Ψ_m) is necessary for maintaining mitochondrial function.^{44,45} In our study, AOPP stimulation significantly decreased Ψ_m and increased mitochondrial superoxide in osteocytes, which implied that mitochondrial dysfunction is induced by AOPPs. Furthermore, the NOX family of NADPH oxidase also shares the capacity to transport electrons across the plasma membrane and generate ROS.³² It has been previously shown that AOPPs activated NADPH oxidase to induce ROS generation in osteoblasts.²² The current study demonstrated that AOPPs upregulate the expression of NOX2 and NOX4, and that apocynin, a NADPH oxidase inhibitor, inhibits AOPP-induced ROS generation, which indicated that activation of NADPH oxidase in osteocytes is induced by AOPPs. Importantly, antioxidant treatment such as apocynin, mito-TEMPO, and NAC reverse the AOPP-induced degeneration of the osteocyte network, decrease of Cx43 expression, and impairment of osteocyte GJIC. Interestingly, we observed that NAC had a better reversal effect in osteocyte GJIC than apocynin and mito-TEMPO, which may be due to the fact that NAC is a non-selective ROS scavenger and has a better scavenging effect on the generation of ROS induced by AOPPs. Therefore, AOPPs induce the activation of NADPH oxidase and mitochondrial dysfunction, and ROS signalling is involved in AOPP-induced impairment of GJIC in osteocytes.

Both ageing and oestrogen deficiency contribute to bone loss in female osteoporotic patients.⁴⁶ Therefore, in order to exclude the interference of oestrogen deficiency, male mice were used as experimental subjects in this study. A previous study demonstrated the age-related degeneration of the osteocyte network and bone microarchitecture in both male and female mice.⁸ The effect of AOPP accumulation on the osteocyte network in aged female mice remains to be further investigated.

In conclusion, our study shows that the accumulation of AOPPs is related to impairment of osteocyte GJIC and bone loss during ageing. AOPPs induce degeneration of the osteocyte network, decrease Cx43 expression,

and impair GJIC in the osteocytes of male mice. AOPP-induced impairment of GJIC in osteocytes is mediated by ROS generation and redox imbalance. Therefore, reducing AOPP accumulation and its cascading effect may be helpful for ameliorating age-related impairment of osteocyte GJIC and bone loss.

Supplementary material



An ARRIVE checklist is included to show that the ARRIVE guidelines were adhered to in this study.

References

1. Tresguerres FGF, Torres J, López-Quiles J, Hernández G, Vega JA, Tresguerres IF. The osteocyte: A multifunctional cell within the bone. *Ann Anat.* 2020;227:151422.
2. Rochefort GY. The osteocyte as a therapeutic target in the treatment of osteoporosis. *Ther Adv Musculoskelet Dis.* 2014;6(3):79–91.
3. Bivi N, Condon KW, Allen MR, et al. Cell autonomous requirement of connexin 43 for osteocyte survival: consequences for endocortical resorption and periosteal bone formation. *J Bone Miner Res.* 2012;27(2):374–389.
4. Maeda S, Tsukihara T. Structure of the gap junction channel and its implications for its biological functions. *Cell Mol Life Sci.* 2011;68(7):1115–1129.
5. Epifantseva I, Shaw RM. Intracellular trafficking pathways of Cx43 gap junction channels. *Biochim Biophys Acta Biomembr.* 2018;1860(1):40–47.
6. Taylor AF, Saunders MM, Shingle DL, Cimbala JM, Zhou Z, Donahue HJ. Mechanically stimulated osteocytes regulate osteoblastic activity via gap junctions. *Am J Physiol Cell Physiol.* 2007;292(1):C545–52.
7. Davis HM, Pacheco-Costa R, Atkinson EG, et al. Disruption of the Cx43/miR21 pathway leads to osteocyte apoptosis and increased osteoclastogenesis with aging. *Ageing Cell.* 2017;16(3):551–563.
8. Tiede-Lewis LM, Xie Y, Hulbert MA, et al. Degeneration of the osteocyte network in the C57BL/6 mouse model of aging. *Ageing (Albany NY).* 2017;9(10):2190–2208.
9. Kar R, Riquelme MA, Werner S, Jiang JX. Connexin 43 channels protect osteocytes against oxidative stress-induced cell death. *J Bone Miner Res.* 2013;28(7):1611–1621.
10. Tiede-Lewis LM, Dallas SL. Changes in the osteocyte lacunocanalicular network with aging. *Bone.* 2019;122:101–113.
11. Donahue HJ, Qu RW, Genetos DC. Joint diseases: from connexins to gap junctions. *Nat Rev Rheumatol.* 2017;14(1):42–51.
12. Batra N, Kar R, Jiang JX. Gap junctions and hemichannels in signal transmission, function and development of bone. *Biochim Biophys Acta.* 2012;1818(8):1909–1918.
13. Stewart S, Darwood A, Masouros S, Higgins C, Ramasamy A. Mechanotransduction in osteogenesis. *Bone Joint Res.* 2020;9(1):1–14.
14. Stains JP, Civitelli R. Gap junctions in skeletal development and function. *Biochim Biophys Acta.* 2005;1719(1–2):69–81.
15. Beyer EC, Berthoud VM. Gap junction gene and protein families: Connexins, innexins, and pannexins. *Biochim Biophys Acta Biomembr.* 2018;1860(1):5–8.
16. Lloyd SA, Loisel AE, Zhang Y, Donahue HJ. Shifting paradigms on the role of connexin43 in the skeletal response to mechanical load. *J Bone Miner Res.* 2014;29(2):275–286.
17. Hua R, Zhang J, Riquelme MA, Jiang JX. Connexin gap junctions and hemichannels link oxidative stress to skeletal physiology and pathology. *Curr Osteoporos Rep.* 2021;19(1):66–74.
18. Loisel AE, Jiang JX, Donahue HJ. Gap junction and hemichannel functions in osteocytes. *Bone.* 2013;54(2):205–212.
19. Cristani M, Speciale A, Saija A, Gangemi S, Minciullo PL, Cimino F. Circulating advanced oxidation protein products as oxidative stress biomarkers and progression mediators in pathological conditions related to inflammation and immune dysregulation. *Curr Med Chem.* 2016;23(34):3862–3882.
20. Maciejczyk M, Zalewska A, Ładny JR. Salivary antioxidant barrier, redox status, and oxidative damage to proteins and lipids in healthy children, adults, and the elderly. *Oxid Med Cell Longev.* 2019;2019:4393460.
21. Wu Q, Zhong Z-M, Pan Y, et al. Advanced oxidation protein products as a novel marker of oxidative stress in postmenopausal osteoporosis. *Med Sci Monit.* 2015;21:2428–2432.
22. Zhu S-Y, Zhuang J-S, Wu Q, et al. Advanced oxidation protein products induce pre-osteoblast apoptosis through a nicotinamide adenine dinucleotide phosphate

- oxidase-dependent, mitogen-activated protein kinases-mediated intrinsic apoptosis pathway. *Aging Cell*. 2018;17(4):e12764.
23. **Zhong ZM, Bai L, Chen JT.** Advanced oxidation protein products inhibit proliferation and differentiation of rat osteoblast-like cells via NF-kappaB pathway. *Cell Physiol Biochem*. 2009;24(1–2):105–114.
 24. **Liu J, Wen S, Lin Y, et al.** Advanced oxidation protein products change biological behaviors of rat endometrial epithelial cells by activating ERK/P38 signaling pathways. *Biol Open*. 2020;9(5):bio048876.
 25. **Liao C-R, Wang S-N, Zhu S-Y, et al.** Advanced oxidation protein products increase TNF- α and IL-1 β expression in chondrocytes via NADPH oxidase 4 and accelerate cartilage degeneration in osteoarthritis progression. *Redox Biol*. 2020;28:101306.
 26. **Lou A, Wang L, Lai W, et al.** Advanced oxidation protein products induce inflammatory responses and invasive behaviour in fibroblast-like synoviocytes via the RAGE-NF- κ B pathway. *Bone Joint Res*. 2021;10(4):259–268.
 27. **Liao Y, Xu J, Qin B, et al.** Advanced oxidation protein products impair autophagic flux in macrophage by inducing lysosomal dysfunction via activation of PI3K-Akt-mTOR pathway in Crohn's disease. *Free Radic Biol Med*. 2021;172:33–47.
 28. **Witko-Sarsat V, Friedlander M, Nguyen Khoa T, et al.** Advanced oxidation protein products as novel mediators of inflammation and monocyte activation in chronic renal failure. *J Immunol*. 1998;161(5):2524–2532.
 29. **Storlino G, Colaiani G, Sanesi L, et al.** Irisin Prevents Disuse-Induced Osteocyte Apoptosis. *J Bone Miner Res*. 2020;35(4):766–775.
 30. **Liu W, Zhang D, Li X, et al.** TGF- β 1 facilitates cell-cell communication in osteocytes via connexin43- and pannexin1-dependent gap junctions. *Cell Death Discov*. 2019;5:141.
 31. **Schell JC, Wisidagama DR, Bensard C, et al.** Control of intestinal stem cell function and proliferation by mitochondrial pyruvate metabolism. *Nat Cell Biol*. 2017;19(9):1027–1036.
 32. **Bedard K, Krause KH.** The NOX family of ROS-generating NADPH oxidases: physiology and pathophysiology. *Physiol Rev*. 2007;87(1):245–313.
 33. **Jensen PK.** Antimycin-insensitive oxidation of succinate and reduced nicotinamide-adenine dinucleotide in electron-transport particles. II. Steroid effects. *Biochim Biophys Acta*. 1966;122(2):167–174.
 34. **Li S, Mao Y, Zhou F, Yang H, Shi Q, Meng B.** Gut microbiome and osteoporosis: a review. *Bone Joint Res*. 2020;9(8):524–530.
 35. **Raina DB, Liu Y, Jacobson OLP, Tanner KE, Tägil M, Lidgren L.** Bone mineral as a drug-seeking moiety and a waste dump. *Bone Joint Res*. 2020;9(10):709–718.
 36. **Nielsen MS, Axelsen LN, Sorgen PL, Verma V, Delmar M, Holstein-Rathlou N-H.** Gap junctions. *Compr Physiol*. 2012;2(3):1981–2035.
 37. **Yu H, Ye W, Zhong Z, Ding R, Chen J.** Effect of advanced oxidation protein products on articular cartilage and synovium in a rabbit osteoarthritis model. *Orthop Surg*. 2015;7(2):161–167.
 38. **Tu C, Wu D-Z, Huang Y-S, et al.** Oxidative Stress Contributes to Hyperalgesia in Osteoporotic Mice. *J Pain Res*. 2020;13:131–142.
 39. **Ding R, Jiang H, Sun B, et al.** Advanced oxidation protein products sensitized the transient receptor potential vanilloid 1 via NADPH oxidase 1 and 4 to cause mechanical hyperalgesia. *Redox Biol*. 2016;10:1–11.
 40. **Riquelme MA, Cardenas ER, Xu H, Jiang JX.** The Role of Connexin Channels in the Response of Mechanical Loading and Unloading of Bone. *Int J Mol Sci*. 2020;21(3):E1146.
 41. **Li R, Jia Z, Trush MA.** Defining ROS in biology and medicine. *React Oxyg Species (Apex)*. 2016;1(1):9–21.
 42. **Zhang YB, Zhong ZM, Hou G, Jiang H, Chen JT.** Involvement of oxidative stress in age-related bone loss. *J Surg Res*. 2011;169(1):e37–42.
 43. **Omidifar N, Moghadami M, Mousavi SM, et al.** Trends in Natural Nutrients for Oxidative Stress and Cell Senescence. *Oxid Med Cell Longev*. 2021;2021:7501424.
 44. **Teodoro JS, Palmeira CM, Rolo AP.** Mitochondrial membrane potential ($\Delta\Psi$) fluctuations associated with the metabolic states of mitochondria. *Methods Mol Biol*. 2018;1782:109–119.
 45. **Boengler K, Kosiol M, Mayr M, Schulz R, Rohrbach S.** Mitochondria and ageing: role in heart, skeletal muscle and adipose tissue. *J Cachexia Sarcopenia Muscle*. 2017;8(3):349–369.
 46. **Khosla S, Oursler MJ, Monroe DG.** Estrogen and the skeleton. *Trends Endocrinol Metab*. 2012;23(11):576–581.

Author information:

- C. Tu, PhD student
- Z. Huang, MD, PhD student
- G. Cai, MD, Doctor
- K. Zhao, MD, PhD student
- J. Gao, MD, PhD student
- Z. Zhong, MD, PhD, Professor
Division of Spine Surgery, Department of Orthopaedics, Nanfang Hospital, Southern Medical University, Guangzhou, China.
- S. Lai, MD, Doctor, Department of Pathology, Nanfang Hospital, Southern Medical University, Guangzhou, China.
- Z. Wu, MD, PhD, Professor, College of Traditional Chinese Medicine, Southern Medical University, Guangzhou, China.

Author contributions:

- C. Tu: Conceptualization, Data curation, Formal analysis, Methodology, Validation, Visualization, Writing – original draft.
- S. Lai: Data curation, Formal Analysis, Writing – original draft.
- Z. Huang: Investigation, Supervision.
- G. Cai: Formal Analysis.
- K. Zhao: Formal Analysis.
- J. Gao: Formal Analysis.
- Z. Wu: Supervision.
- Z. Zhong: Conceptualization, Funding acquisition, Supervision, Writing – review & editing.

Funding statement:

- The authors disclose receipt of the following financial or material support for the research, authorship, and/or publication of this article: this work was supported in part by the National Natural Science Foundation of China (No.81871819) and the Natural Science Foundation of Guangdong Province (No. 2019A1515012075).

ICMJE COI statement:

- Each author certifies that neither they nor immediate family has any funding or commercial associations, related or unrelated to this study (e.g. consultancies, stock ownership, equity interest, patent/licensing arrangements, etc.).

Ethical review statement:

- All animal experiments were approved by the Laboratory Animal Care and Use Committee of Nanfang Hospital, Southern Medical University (No. NFYY-2020-0261).

Open access funding

- We received open access funding for this manuscript from the National Natural Science Foundation of China (No. 81871819).

© 2022 Author(s) et al. This is an open-access article distributed under the terms of the Creative Commons Attribution Non-Commercial No Derivatives (CC BY-NC-ND 4.0) licence, which permits the copying and redistribution of the work only, and provided the original author and source are credited. See <https://creativecommons.org/licenses/by-nc-nd/4.0/>